RSC Advances

PAPER

View Article Online
View Journal | View Issue

Published on 23 February 2015. Downloaded by University of California - San Diego on 12/03/2015 09:13:52.

Cite this: *RSC Adv.*, 2015, **5**, 24319

A polyoxometalate-assisted approach for synthesis of Pd nanoparticles on graphene nanosheets: synergistic behaviour for enhanced electrocatalytic activity†

Sara Khadempir,[a] Ali Ahmadpour,*[a] Mohammad T. Hamed Mosavian,[a] Narges Ashraf,[b] Fatemeh F. Bamoharram,[c] Scott G. Mitchell[d] and Jesús M. de la Fuente[de]

Received 19th January 2015
Accepted 23rd February 2015

DOI: 10.1039/c5ra01084e

www.rsc.org/advances

A polyoxometalate (POM) assisted approach has been employed to prepare a nanohybrid of Pd nanoparticles (PdNPs) and graphene nanosheets (GNSs). The Keggin-type POM, phosphomolybdic acid (PMo_{12}), was applied to serve as both reducing and stabilising agent. The as-prepared nanohybrid (Pd/PMo_{12}/GNSs) was comprehensively characterised using transmission electron microscopy and X-ray diffraction analysis. The synergistic behaviour of PdNPs, PMo_{12} and GNSs in the nanohybrid leads to elevated electrocatalytic property for ethanol oxidation. Moreover, the Pd/PMo_{12}/GNSs nanohybrid was activated by applying a sufficiently negative potential which plays a key role in promoting the electrocatalytic activity. The activated catalyst presents a superior performance towards ethanol electrooxidation reaction and shows better tolerance to poisoning species compared to Pd and Pt nanoparticles. The outstanding electrocatalytic activity of the tri-component (Pd/PMo_{12}/GNSs) nanohybrid is discussed with relevance to its application in direct alcohol fuel cells (DAFCs).

Introduction

Direct alcohol fuel cells (DAFCs) are regarded as attractive future power sources due to their high energy density, low pollutant emission, ease of handling, portable applications and low operating temperature.[1–4] Various alcohols such as methanol, ethanol, ethylene glycol, glycerol and so forth have been widely investigated for their potential applications as fuels.[5–8] Among the different types of DAFCs, there is a special interest in direct ethanol fuel cells, since ethanol is not toxic and it can easily be prepared in large amounts by fermentation of sugar-containing raw materials.[9–11]

Pt-based catalysts are employed extensively for oxidation of alcohols in DAFCs; however, the high cost, finite resources and poisoning of Pt catalysts – particularly in alkaline media – restrict commercialisation of DAFCs. The efficiency of fuel cells can be improved significantly in alkaline media; therefore, the quest for a suitable Pt-free catalyst to be used in this media is still progressing.[1,11–13]

As a result, Pd-based catalysts have recently been introduced as an alternative choice. Application of palladium nanoparticles (PdNPs) – as opposed to bulk Pd metal – allows synthesis of a highly efficient catalyst using only a very small amount of this material. PdNPs are one of the most useful catalysts for oxidation of small organic molecules and they have reportedly higher electrocatalytic activity towards ethanol oxidation compared with that of PtNPs; especially in alkaline media.[4,14–16] Besides, the abundance of Pd on the earth crust is at least fifty times more than that of Pt.[11,15] Furthermore, the application of PdNP hybrids is of considerable interest, since the dispersion of PdNPs in a proper conductive support such as carbon would minimise the aggregation of PdNPs; while at the same time maximise their electrocatalytic activity.

Graphene is a two-dimensional carbon material that shows some exceptional properties such as high electrical conductivity, large specific surface area and superior electron mobility, making it an ideal support material for catalytically active metal NPs.[17,18] Although there are several approaches to load metal NPs on graphene nanosheets (GNSs), developing simple and effective methods that produce well-dispersed NPs without using hazardous/toxic organic reagents are most desirable.

Polyoxometalates (POMs) are early-row transition metal oxygen anionic clusters with a remarkable and diverse range of

[a]Department of Chemical Engineering, Faculty of Engineering, Ferdowsi University of Mashhad, Mashhad, Iran. E-mail: ahmadpour@um.ac.ir
[b]Department of Chemistry, Faculty of Sciences, Ferdowsi University of Mashhad, Mashhad, Iran
[c]Department of Chemistry, Mashhad Branch, Islamic Azad University, Mashhad, Iran
[d]Instituto de Nanociencia de Aragon (INA), Universidad de Zaragoza, 50018-Zaragoza, Spain
[e]Instituto de Ciencia de Materiales de Aragón (ICMA), CSIC-Universidad de Zaragoza, C/Pedro Cerbuna 12, 50009-Zaragoza, Spain

† Electronic supplementary information (ESI) available. See DOI: 10.1039/c5ra01084e

Published on 23 February 2015. Downloaded by University of California - San Diego on 12/03/2015 09:13:52.

redox and photo-electrochemical properties.[19–22] POMs have been utilised in the preparation of metal NPs/POM/GNSs nanohybrids, since they can act as both reducing and stabilising molecules for metal NPs.[23–25] Liu and co-workers have reported the synthesis of Au, Pd and PtNPs on GNSs using phosphotungstic acid, $H_3PW_{12}O_{40}$, for biosensing applications and the electrooxidation of formic acid and methanol in acidic media, respectively.[26–29]

Herein, we report how the Keggin-type POM phosphomolybdic acid ($H_3PMo_{12}O_{40}$, herein PMo_{12}) was employed to prepare well-dispersed POM-stabilised PdNPs on GNSs. The electrocatalytic activity of the tri-component nanohybrid was then tested and was found to be an efficient catalyst for ethanol electrooxidation. Also, an activation step has been proposed to enhance the electrocatalytic activity of the tri-component Pd/PMo_{12}/GNSs nanohybrid. In summary, this easy-to-prepare nanohybrid shows to be a promising catalyst for ethanol electrooxidation in alkaline media.

Experimental

Chemicals and reagents

All chemicals were of analytical grade purity and used as received without any purification. Palladium(II) chloride ($PdCl_2$), isopropyl alcohol, sodium hydroxide (NaOH), potassium permanganate ($KMnO_4$), hydrogen peroxide (H_2O_2) and graphite powder (<50 μm) were purchased from Merck (Darmstadt, Germany). Functionalised Multi Walled Carbon Nanotubes (CNTs, >95%, OD: 5–15 nm, US NANO). $H_3PMo_{12}O_{40}$ (PMo_{12}) was purchased from Sigma-Aldrich. Phosphate buffer solution (0.1 M) was prepared by dissolving the proper amount of $NaH_2PO_4 \cdot 2H_2O$ (Merck, Darmstadt, Germany) in deionised water and adjusting the pH to 8.5 by 0.1 M NaOH solution. Deionised (DI) water (18.3 MΩ cm) was used throughout the entire work.

Synthesis of graphene oxide (GO)

GO was prepared by pre-oxidation of graphite which was followed by post-oxidation with Hummers method.[30,31]

In the pre-oxidation step, the graphite powder (2.0 g) was added to the mixed solution of H_2SO_4 99.97% (20 mL), $K_2S_2O_8$ (1.0 g) and P_2O_5 (1.0 g). The mixture was reacting at 80 °C for 4.5 h; after which, it was cooled and diluted with 1 L of DI water and left overnight. Then, it was filtered, washed and dried in air. In the post-oxidation step, the pre-oxidised graphite (0.5 g) was dispersed into a chilled mixture of $NaNO_3$ (0.5 g) and H_2SO_4 (23 mL) in an ice bath. Thereafter, $KMnO_4$ (10 g) was added slowly while the solution was stirring and the temperature maintained down to 20 °C. The mixture was kept at 35 °C for 2 h, after which DI water (140 mL) was added with controlling the temperature below 50 °C to give a dark brown solution. In order to stop the reaction, 2 mL of H_2O_2 were added and the reaction was allowed to settle overnight. After centrifuging and washing with hydrochloric acid and DI water, the resulting solid was air-dried. DI water was then added and the GO was resuspended using ultrasonication. It is notable that the GO dispersion was found to be stable for several months. The resulting homogenous brown GO was dried in air.

Synthesis of Pd/PMo_{12}/GNSs

In a typical synthesis, 3.6 mg $PdCl_2$ and 28.4 mg PMo_{12} were added to 100 mL DI water and completely dissolved. Then, 9.6 mL of the as-prepared solution was transformed to a spectrophotometer cell, 460 μg GO was added to the mixture and ultrasonicated for 20 min. Thereafter, the mixture was deoxygenated with N_2 gas, and 0.4 mL isopropyl alcohol were added to the mixture and it was irradiated under a UV lamp (125 W high pressure mercury vapour lamp) for 2 h under continuous stirring. The reaction was performed at a constant room temperature using water circulating system. After the photocatalytic Pd reduction process, the mixture was centrifuged at 14 000 rpm for 10 min, and then dried at 50 °C overnight. By adjusting the amount of GO, different loadings of PdNPs on GNSs (15, 30 and 45 wt%) were obtained. The Pd/PMo_{12}/CNTs nanohybrid was synthesised with the same procedure by substituting of GO with CNTs. The Pd/GNSs were prepared using a procedure from the literature.[32]

Apparatus

High-resolution transmission electron microscopy (HRTEM) and high-angle annular dark field-scanning transmission electron microscopy (HAADF-STEM) images were acquired using a Tecnai S-Twin30, 300 keV, GIF-TRIDIEM. Energy-dispersive X-ray spectroscopy (EDS) data were obtained on the same instrument. Scanning electron microscopy (SEM) images were acquired using a field emission SEM Inspect F50 with an EDX system INCA PentaFETx3 (FEI Company, Eindhoven, Netherlands) in an energy range between 0–30 keV. TEM observation was obtained on a CM120, Philips transmission electron microscope and X-ray diffraction (XRD) analysis was carried out using the X'Pert Pro MPD diffractometer.

All the electrochemical experiments were carried out using a μ-Autolab type III electrochemical workstation with a conventional three-electrode setup. A glassy carbon electrode (GC, 2 mm in diameter, Azar electrode Co.) was used as working electrode. A platinum wire and a saturated Ag/AgCl electrode (both from Azar electrode Co.) were used as counter and reference electrodes, respectively.

Electrochemical experiments

The modified electrode was prepared by the following procedures: (a) GC electrode was polished thoroughly by 0.5 μm alumina slurry and was washed with water and acetone; (b) a catalyst solution (1.0 mg mL^{-1}) was prepared by sonicating the as-prepared catalyst and proper amount of DI water; and (c) 2 μL of catalyst solution was dropped onto the surface of the prepolished GC electrode and dried in air. All experiments were performed at room temperature.

 This journal is © The Royal Society of Chemistry 2015

Published on 23 February 2015. Downloaded by University of California - San Diego on 12/03/2015 09:13:52.

Results and discussion

Structural analysis

The morphology and microstructure of the Pd/PMo_{12}/GNSs nanohybrids were investigated by TEM and SEM.

Fig. 1 shows typical TEM images of the 30% Pd/PMo_{12}/GNSs with different magnifications. From Fig. 1a it can be observed that the GNSs were covered homogeneously with PdNPs. From Fig. 1b, it is seen that small well-defined spherical PdNPs are dispersed homogeneously on the surface of the GNSs, with the

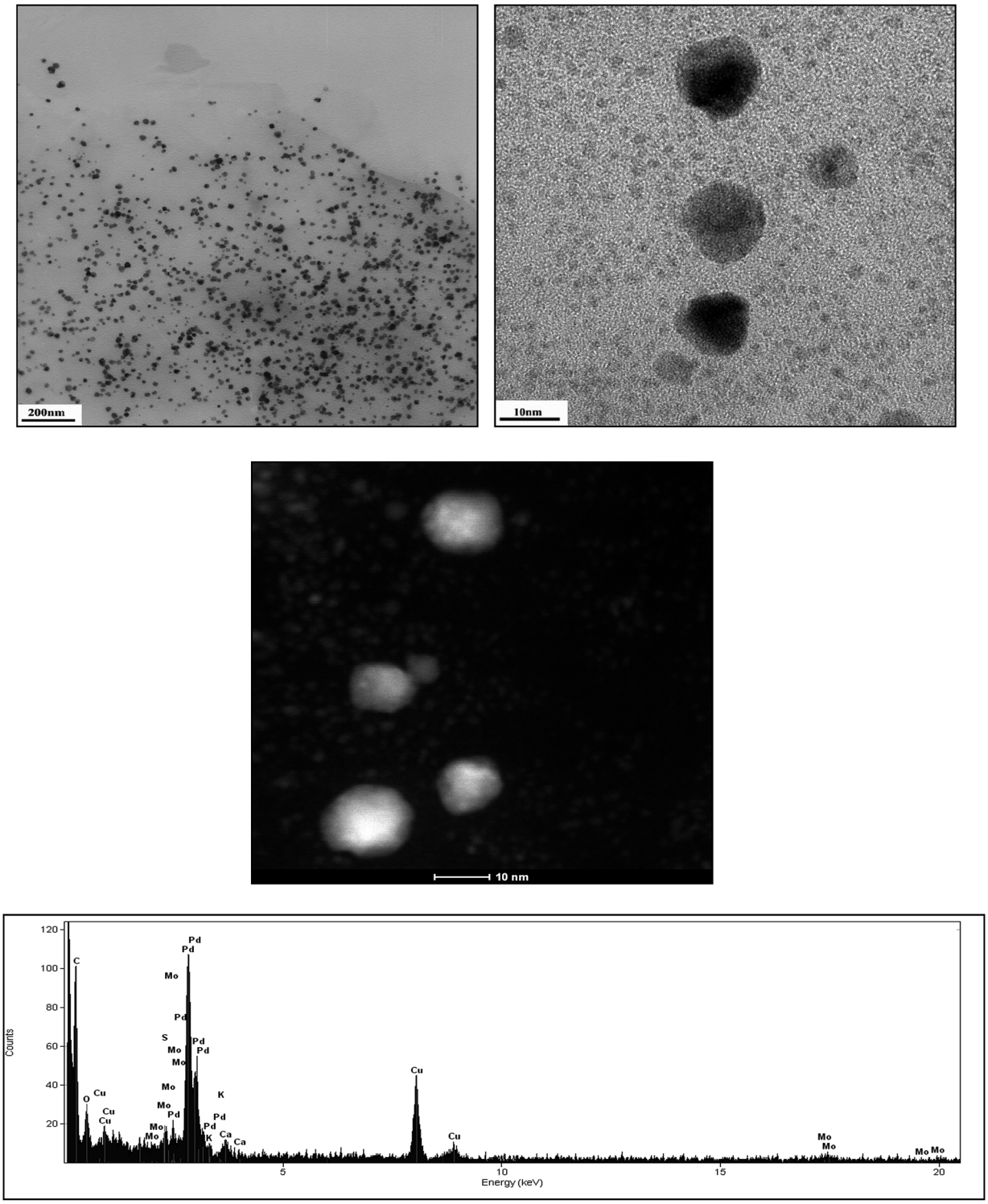

Fig. 1 (a and b) TEM images of Pd/PMo_{12}/GNSs with different magnifications; (c) HAADF-STEM image of 30% Pd/PMo_{12}/GNSs (d) the corresponding EDS analysis.

Published on 23 February 2015. Downloaded by University of California - San Diego on 12/03/2015 09:13:52.

exception of some large PdNPs. It looks like there may be two size dispersions of the PdNPs. It is noted that the PdNPs preferentially attached to the surfaces of GNSs, rather than in the regions without GNSs (Fig. S1†). A typical HAADF-STEM image (Fig. 1c) and coupled EDS analysis (Fig. 1d) showed that strong molybdenum peaks exist except the palladium peaks, confirming the existence of the PMo_{12} in the hybrid. The as-prepared nanohybrid consists mainly of carbon with an amount of oxygen from PMo_{12} frame and probably due to the presence of traced unreduced oxygen-containing groups on the surface of GNSs. The strong peaks of Cu originate from the copper TEM grid. Fig. S2 and S3† represent the TEM and HAADF-STEM images of samples with 15 and 45% Pd loadings. These images indicate good contrast for the PdNPs in 15% loading. For 45% loading a significant increase in the amount of PdNPs on GNSs can be observed; these particles are much more aggregated (*i.e.* less discrete particles) and they appear to be of more irregular shape.

SEM images of samples with different loadings of PdNPs (Fig. S4†) show the dispersion of PdNPs on the surface of transparent thin and sleek crumpled graphene sheets and confirm the TEM results.

The XRD patterns of the GO and 30% Pd/PMo_{12}/GNSs are shown in Fig. 2. The graphite pattern (not shown) reveals a sharp diffraction peak at $2\theta = 26.7°$ corresponding to (002) planes with *d*-spacing of 3.34 Å. As shown in the XRD pattern of GO, the disappearance of the graphite diffraction peak at about 26.7° and appearance of new peak in 9.27° corresponding to the interlayer spacing of 9.53 Å revealed the successful oxidation of the graphite. In addition, the increases in *d* value of GO compared to graphite shows that the distance between the carbon sheets has increased due to the insertion of interplanar oxygen-containing functional groups. After the reduction of GO and $PdCl_2$ by PMo_{12}-assisted photoreduction process, the disappearance of the peak at $2\theta = 9.27°$ confirms that oxygen groups have been removed and GO has been flaked and reduced to GNSs;[33] also the strong diffraction peaks at $2\theta = 40.02°$, 46.59° and 68.08° indicate PdNPs formation and assigned to the (111), (200) and (220) crystalline planes of the face-centered cubic (fcc) structures Pd (JCPDS no. 46-1043), respectively.[34] These diffraction peaks were observed to be sharp with a high intensity indicating high crystallinity of Pd. Besides, since there are no noticeable diffraction peaks in the measurement that correspond to the crystallised PMo_{12} or Mo oxides, it can be concluded that the PMo_{12} is adsorbed in a highly dispersed manner on the catalyst with no agglomeration.[35]

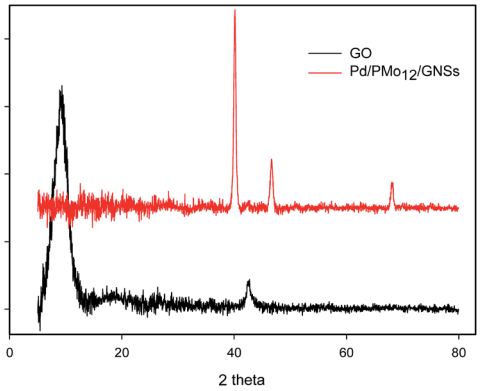

Fig. 2 XRD pattern of GO (bottom) and 30% Pd/PMo_{12}/GNSs (top).

Electrochemical characterisation of Pd/PMo_{12}/GNSs nanohybrid

To investigate the electrochemical performance of Pd/PMo_{12}/GNSs nanohybrid and its catalytic behaviour towards electro-oxidation of ethanol, cyclic voltammetry (CV) experiments were performed.

Electrocatalytic oxidation of ethanol

Electrocatalytic oxidation of ethanol was studied at the pure PdNPs and the Pd/PMo_{12}/GNSs modified GC with different loadings (15, 25, 30 and 45%) of Pd on GNSs in the solution of 1.0 M NaOH and 1.0 M ethanol at room temperature (Fig. 3).

Each CV curve was characterised by two well-defined anodic (oxidation) current peaks. The peak in the forward scan direction was assigned to the oxidation of freshly chemisorbed ethanol and the peak in reverse scan direction corresponds to the oxidation of residual carbonaceous species formed in the forward scan.[36] As shown in Fig. 3, the electrocatalytic oxidation of the as-prepared catalysts is enhanced by increasing the PdNPs loading up to 30% and then declined with further increasing in loading due to the agglomerations of PdNPs. As a result, 30% loading of PdNPs on GNSs and CNTs were used for further studies.

The electrocatalytic oxidation of ethanol was studied by Pd/PMo_{12}/GNSs and Pd/PMo_{12}/CNTs (Fig. 4) and the results are shown in Table 1.

It should be noted that ethanol electrooxidation peak in back-ward scan was observed at −0.4 V for Pd/PMo_{12}/GNSs, which indeed occurs at the potential near the reduction peak potential for oxygenated species on Pd surface (*i.e.* −0.4 V) as shown by the insert in Fig. 4.

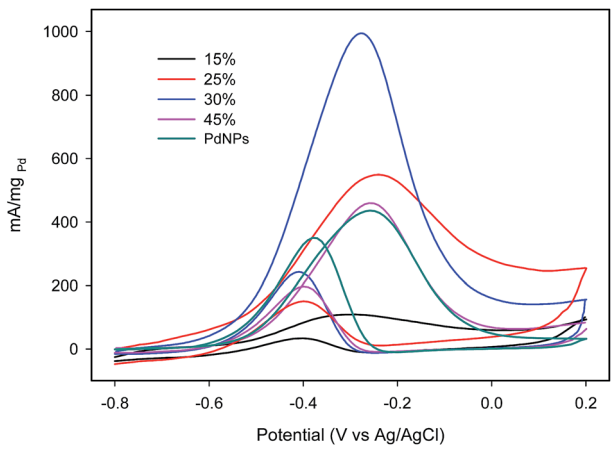

Fig. 3 Cyclic voltammograms (CV) in 1.0 M NaOH and 1.0 M ethanol solution, scan rate: 50 mV s^{-1} for Pd/PMo_{12}/GNSs at different loading and for pure PdNPs.

 This journal is © The Royal Society of Chemistry 2015

Published on 23 February 2015. Downloaded by University of California - San Diego on 12/03/2015 09:13:52.

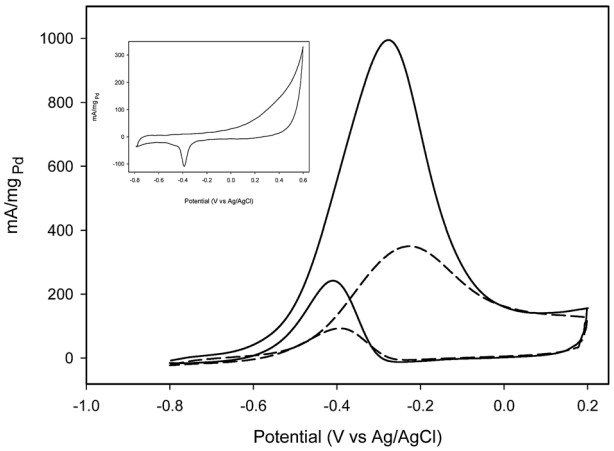

Fig. 4 Cyclic voltammograms (CV) in 1.0 M NaOH with 1.0 M ethanol, scan rate: 50 mV s^{-1} for Pd/PMo_{12}/GNSs (solid line) and for Pd/PMo_{12}/CNTs (dashed line). Insert: (CV) curve in the absence of ethanol.

The forward peak mass current density (J_f) for the Pd/PMo_{12}/GNSs is considerably higher than that of the Pd/PMo_{12}/CNTs which shows the superior performance of the GNSs as support. In comparison with CNTs, GNSs have a larger specific surface area, thereby providing much more accessible sites for uniform dispersion of PdNPs and improving catalytic activity.

In addition, the ratio of the forward oxidation peak current (I_f) to the backward oxidation peak current (I_b), I_f/I_b, is an important criterion for comparing the performance of the catalysts. The higher value of I_f/I_b, implies that the catalyst has greater catalytic activity and better tolerance to carbonaceous species accumulation. The I_f/I_b for Pd/PMo_{12}/GNSs (*i.e.* 4.1) is higher than that of Pd/PMo_{12}/CNTs (3.7) and even significantly greater than the values reported in the literatures.[4,12,37]

The other considerable evidence is that the onset potential for Pd/PMo_{12}/GNSs is more negative than Pd/PMo_{12}/CNTs. It reveals that electrooxidation of ethanol with GNSs support is more facile than CNTs.

For comparison, the activity of graphene oxide toward ethanol electrooxidation is presented in Fig. S5.† As shown in this figure, the graphene oxide has no catalytic activity.

Electrochemical active surface area (ECSA)

It is well known that electrochemical active surface area (ECSA) is measured using cyclic voltammogram of the catalysts in NaOH or H_2SO_4 solution. In the case of Pt-based catalysts, the charge of a monolayer of adsorbed hydrogen is used to evaluate the ECSA. However, for Pd-based catalysts, due to the strong affinity of Pd towards hydrogen adsorption, it is difficult to determine a monolayer of adsorbed hydrogen. Therefore, ECSA is measured through the reduction peak of palladium oxide in NaOH solution.[4] The CV of the as-prepared catalyst in N_2-saturated 1.0 M NaOH solution is shown in Fig. 5.

The ECSA is calculated from eqn (1):

$$\mathrm{ECSA} = \frac{Q}{Sl} \tag{1}$$

where "*S*" is the proportionally constant used to relate charge with area, "*l*" is the catalyst loading in gram, and "*Q*" is the columbic charge for the reduction of palladium oxide, which was determined by the integration of area under the oxide reduction peak. A charge value of 4.05 cm^{-2} was assumed for the reduction of palladium oxide monolayer The ECSA not only provides the data about active surface area but also gives important information about the selection of electrocatalytic support. The calculated values of ECSA for Pd/PMo_{12}/GNSs and Pd/PMo_{12}/CNTs catalysts were 38.67 and 26.3 m^2 g^{-1}, respectively. The results confirm the better performance of GNSs support compared to CNTs.

Electrochemical behaviour of immobilized PMo_{12}

To prove the presence of PMo_{12} in the structure of the as-prepared catalyst, the CVs of Pd/PMo_{12}/GNSs and Pd/GNSs were recorded in N_2-saturated 1.0 M H_2SO_4 solution which have been indicated in Fig. 6. Comparison of the CVs of Pd/PMo_{12}/GNSs and Pd/GNSs shows that oxidation and reduction peaks appearing at about 0.00 and 0.1 V could be attributed to

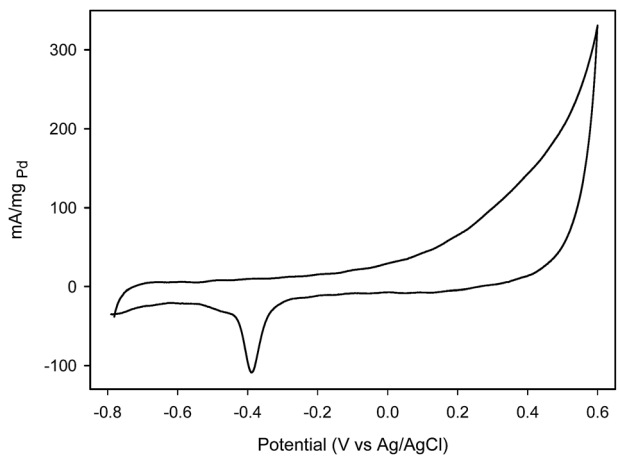

Fig. 5 Cyclic voltammogram (CV) of Pd/PMo_{12}/GNSs in 1.0 M NaOH solution, scan rate: 50 mV s^{-1}.

Table 1 Ethanol electrooxidation properties of Pd/PMo_{12}/GNSs and Pd/PMo_{12}/CNTs

	E_{op}[a] (V)	J_f (mA mg_{Pd}^{-1} cm^{-2})	E_f[b] (V)	J_b (mA mg_{Pd}^{-1} cm^{-2})	E_b[c] (V)	I_f/I_b
Pd/PMo_{12}/GNSs	−0.68	31 668	−0.275	7722	−0.409	4.1
Pd/PMo_{12}/CNTs	−0.57	11 154	−0.223	2967	−0.392	3.7

[a] E_{op} = onset potential. [b] E_f = forward peak current potential. [c] E_b = backward peak current potential.

Published on 23 February 2015. Downloaded by University of California - San Diego on 12/03/2015 09:13:52.

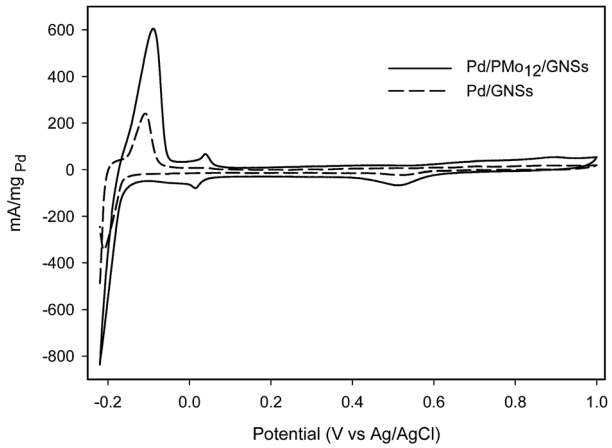

Fig. 6 Cyclic voltammograms (CV) of Pd/PMo_{12}/GNSs (solid line) and Pd/GNSs (dashed line) in 1.0 M H_2SO_4 solution, scan rate: 50 mV s^{-1}.

the presence of PMo_{12}. Obviously, the peaks at potentials more negative than −0.05 V correspond to hydrogen evolution, proton discharge.

Furthermore, the CVs of Pd/PMo_{12}/GNSs in 1.0 M H_2SO_4 solution at different scan rates and the insert shows that the $i_{p,a}$ and the $i_{p,c}$ for the attributed oxidation and reduction peaks of PMo_{12}, are linear *versus* scan rates, indicating a surface-controlled redox process for PMo_{12} adsorbed on the surface of PdNPs and GNSs (Fig. 7).[38,39]

To investigate the mechanism of the electrocatalytic oxidation of ethanol, cyclic voltammograms of the prepared catalyst were recorded in three separate alkaline (1.0 M NaOH) solutions containing ethanol, acetaldehyde and potassium acetate (Fig. 8). No oxidation current was observable in the acetate solution; while acetaldehyde showed a considerable oxidation peak. This fact implies that the acetate is the final product and acetaldehyde is an active intermediate which is consistent with the mechanism reported previously in the literatures.[36,40,41] Based on this mechanism, ethanol electrooxidation on Pd

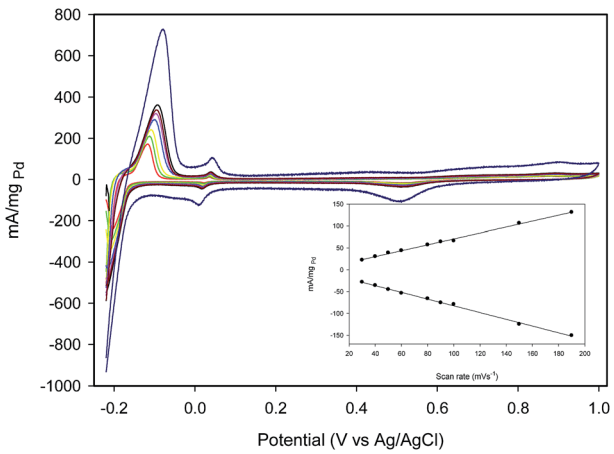

Fig. 7 Cyclic voltammograms (CV) of Pd/PMo_{12}/GNSs in 1.0 M H_2SO_4 solution at different scan rate. Insert: corresponding dependence of the peaks for PMo_{12}.

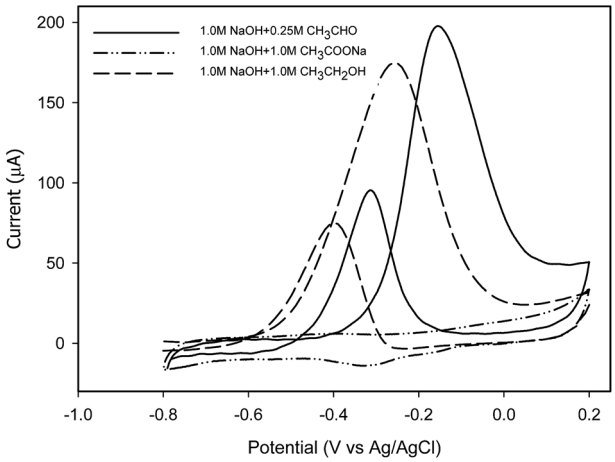

Fig. 8 Cyclic voltammograms (CV) of the Pd/PMo_{12}/GNSs in 1.0 M NaOH solution containing different fuels: ethanol, acetaldehyde and potassium acetate (scan rate: 50 mV s^{-1}).

involves the formation of Pd-$(CH_3CO)_{ads}$ upon C–H cleavage.[40] The successive reactions can be expressed as follows:

$$Pd + CH_3CH_2OH \leftrightarrow Pd\text{-}(CH_3CH_2OH)_{ads} \quad (2)$$

$$Pd\text{-}(CH_3CH_2OH)_{ads} + 3OH^- \rightarrow Pd\text{-}(CH_3CO)_{ads} + 3H_2O + 3e^- \quad (3)$$

$$Pd\text{-}(CH_3CO)_{ads} + Pd\text{-}OH_{ads} \rightarrow Pd\text{-}CH_3COOH + Pd \quad (4)$$

$$Pd\text{-}CH_3COOH + OH^- \rightarrow Pd + CH_3COO^- + H_2O \quad (5)$$

It is noteworthy that the reaction of the Pd-$(CH_3CO)_{ads}$ with the activated Pd-OH_{ads} species is the rate determining step, so the efficiency of the reaction is determined by the degree of CH_3CO_{ads} and OH_{ads} coverage. Formation of Pd-OH_{ads} would take place through the adsorption of hydroxyl groups at the surface of PdNPs at negative potentials as shown by the following equation.[41]

$$Pd + OH^- \rightarrow Pd\text{-}OH_{ads} + e^- \quad (6)$$

This implies that the mass transfer of OH^- to the surface of PdNPs plays an essential role in the efficiency of Pd-OH_{ads} formation. Electrolytic generation of OH^- species adjacent to the surface of PdNPs would promote the reaction efficiency. Electrolysis of water in basic media results in the formation of OH^- species which are readily adsorbed at the surface of neighboring PdNPs. To verify this concept, an activation step has been performed to the surface of electrode by applying a constant potential step of −1.5 V for 300 s duration in phosphate buffer solution (pH = 8.50). As a result, the following reaction would take place at the electrode–electrolyte interface and the Pd-OH_{ads} sites create at the surface of PdNPs.

$$2H_2O + 2e^- \rightarrow H_2(g) + 2OH^- \quad (7)$$

 This journal is © The Royal Society of Chemistry 2015

Published on 23 February 2015. Downloaded by University of California - San Diego on 12/03/2015 09:13:52.

Table 2 Effect of activation step on ethanol electrooxidation

	E_{op} (V)	J_f (mA mg_{Pd}^{-1} cm^{-2})	E_f (V)	J_b (mA mg_{Pd}^{-1} cm^{-2})	E_b (V)	I_f/I_b
Activated Pd/PMo_{12}/GNSs	−0.68	31 668	−0.275	7722	−0.409	4.1
Pd/PMo_{12}/GNSs	−0.53	2341	−0.210	836	−0.300	2.8

Table 2 shows the effect of activation step on the performance of the catalyst towards the catalytic electrooxidation of ethanol. Comparison of the CVs indicates the excellent performance of the activated Pd/PMo_{12}/GNSs catalyst.

Conclusion

We have shown that the tri-component of Pd/PMo_{12}/GNSs nanohybrid can be used as an efficient electrocatalyst for oxidation of ethanol. This material has been prepared using the Keggin-type polyoxometalate phosphomolybdic acid (PMo_{12}) as both a reducing and stabilising agent. A novel method for activation of the catalyst has also been described and the electrochemical investigations here within indicate that this activation process substantially enhances the electrocatalytic activity of the catalyst. Consequently, the as-prepared tri-component nanohybrid catalyst showed a considerably higher electrocatalytic activity towards ethanol oxidation. The superior electrocatalytic performance is a synergic effect resulting principally from: (i) the superior electron mobility of GNSs and ionic conductivity of PMo_{12}; (ii) the small size and high dispersion of PdNPs on the GNS support; (iii) a possible synergic and bifunctional effect between PdNPs and PMo_{12};[42] and (iv) formation of abundant Pd-OH_{ads} sites in the activation step. Moreover, because of the higher ECSA, better tolerance towards poisoning carbonaceous species and improve onset potential, the Pd/PMo_{12}/GNSs shows an enhanced catalytic activity compared to Pd/PMo_{12}/CNTs. In summary, the activated Pd/PMo_{12}/GNSs nanohybrid showed highly promising features for development of Pd-based catalysts to be used in alkaline direct ethanol fuel cells.

Acknowledgements

The authors would like to thank Mrs S. Rajabzade for her help with the electrochemical measurements. TEM, HAADF-STEM measurements have been performed through part of the fund of the Marie Curie Intra-European Fellowship 328985-COCOPOPS and ERC-Starting Grant 239931-NANOPUZZLE. Dr Rodrigo Fernández-Pacheco (LMA-UNIZAR) provided invaluable advice and assistance with the electron microscopy data collection.

References

1 Y. Zhao, L. Zhan, J. Tian, S. Nie and Z. Ning, *Electrochim. Acta*, 2011, **56**, 1967–1972.
2 G. F. Alvarez, M. Mamlouk, S. M. Senthil Kumar and K. Scott, *J. Appl. Electrochem.*, 2011, **41**, 925–937.
3 S. M. Choi, M. H. Seo, H. J. Kim and W. B. Kim, *Carbon*, 2011, **49**, 904–909.
4 L. Gao, W. Yue, S. Tao and L. Fan, *Langmuir*, 2012, **29**, 957–964.
5 R. Kannan, A. Kim and D. Yoo, *J. Appl. Electrochem.*, 2014, **44**, 893–902.
6 A. Santasalo-Aarnio, Y. Kwon, E. Ahlberg, K. Kontturi, T. Kallio and M. T. M. Koper, *Electrochem. Commun.*, 2011, **13**, 466–469.
7 J. L. Dongyao Wang, Z. Wu, J. Zhang, Y. Su, Z. Liu and C. Xu, *Int. J. Electrochem. Sci.*, 2009, **4**, 1672–1678.
8 S. C. Si-Wen Xie, Z.-Q. Liu and C.-W. Xu, *Int. J. Electrochem. Sci.*, 2011, **6**, 882–888.
9 Z. Cui, P. J. Kulesza, C. M. Li, W. Xing and S. P. Jiang, *Int. J. Hydrogen Energy*, 2011, **36**, 8508–8517.
10 X.-M. Chen, Z.-J. Lin, T.-T. Jia, Z.-M. Cai, X.-L. Huang, Y.-Q. Jiang, X. Chen and G.-N. Chen, *Anal. Chim. Acta*, 2009, **650**, 54–58.
11 R. N. Singh, A. Singh and Anintida, *Carbon*, 2009, **47**, 271–278.
12 R. N. Singh and R. Awasthi, *Catal. Sci. Technol.*, 2011, **1**, 778–783.
13 N. Tian, Z.-Y. Zhou, N.-F. Yu, L.-Y. Wang and S.-G. Sun, *J. Am. Chem. Soc.*, 2010, **132**, 7580–7581.
14 C. W. Xu, H. Wang, P. K. Shen and S. P. Jiang, *Adv. Mater.*, 2007, **19**, 4256–4259.
15 P. K. Shen and C. Xu, *Electrochem. Commun.*, 2006, **8**, 184–188.
16 H. Wang, C. Xu, F. Cheng and S. Jiang, *Electrochem. Commun.*, 2007, **9**, 1212–1216.
17 S. Park and R. S. Ruoff, *Nat. Nanotechnol.*, 2009, **4**, 217–224.
18 S. Rajabzadeh, G. Ronagi, M. H. Arbab Zavar and N. Ashraf, *Electrochim. Acta*, 2014, **135**, 543–549.
19 A. Ahmadpour, A. Ayati, H. Rashidi and B. Tanhaei, *Synth. React. Inorg., Met.-Org., Nano-Met. Chem.*, 2012, **42**, 209–230.
20 A. Ahmadpour, B. Tanhaei and A. Ayati, *Curr. Nanosci.*, 2012, **8**, 880–884.
21 A. Ayati and A. Ahmadpour, *Gold Bull.*, 2012, **45**, 145–151.
22 A. Ayati, A. Ahmadpour, H. Rashidi and B. Tanhaei, *Journal of Nanostructure in Chemistry*, 2011, **2**, 15–22.
23 S. G. Mitchell and J. M. de la Fuente, *J. Mater. Chem.*, 2012, **22**, 18091–18100.
24 Y. Wang and I. A. Weinstock, *Chem. Soc. Rev.*, 2012, **41**, 7479–7496.
25 Y.-F. Song and R. Tsunashima, *Chem. Soc. Rev.*, 2012, **41**, 7384–7402.
26 S. Li, X. Yu, G. Zhang, Y. Ma, J. Yao and P. de Oliveira, *Carbon*, 2011, **49**, 1906–1911.

Published on 23 February 2015. Downloaded by University of California - San Diego on 12/03/2015 09:13:52.

27 R. Liu, S. Li, X. Yu, G. Zhang, S. Zhang, J. Yao and L. Zhi, *J. Mater. Chem.*, 2012, **22**, 3319–3322.
28 R. Liu, S. Li, X. Yu, G. Zhang, Y. Ma and J. Yao, *J. Mater. Chem.*, 2011, **21**, 14917–14924.
29 A. Troupis, A. Hiskia and E. Papaconstantinou, *Angew. Chem., Int. Ed.*, 2002, **41**, 1911–1914.
30 W. S. Hummers and R. E. Offeman, *J. Am. Chem. Soc.*, 1958, **80**, 1339.
31 J. K. Lee, K. B. Smith, C. M. Hayner and H. H. Kung, *Chem. Commun.*, 2010, **46**, 2025–2027.
32 X. Chen, G. Wu, J. Chen, X. Chen, Z. Xie and X. Wang, *J. Am. Chem. Soc.*, 2011, **133**, 3693–3695.
33 S. Bai, X. Shen, X. Zhong, Y. Liu, G. Zhu, X. Xu and K. Chen, *Carbon*, 2012, **50**, 2337–2346.
34 J.-J. Shi and J.-J. Zhu, *Electrochim. Acta*, 2011, **56**, 6008–6013.
35 M. H. Seo, S. M. Choi, H. J. Kim, J. H. Kim, B. K. Cho and W. B. Kim, *J. Power Sources*, 2008, **179**, 81–86.
36 J. Yin, S. Shan, M. S. Ng, L. Yang, D. Mott, W. Fang, N. Kang, J. Luo and C.-J. Zhong, *Langmuir*, 2013, **29**, 9249–9258.
37 C. Xu, P. K. Shen and Y. Liu, *J. Power Sources*, 2007, **164**, 527–531.
38 J. Chen, S. Liu, W. Feng, G. Zhang and F. Yang, *Phys. Chem. Chem. Phys.*, 2013, **15**, 5664–5669.
39 J. Yuan, B. He, L. Hong, J. Lu, J. Miao and L. Niu, *J. Mater. Chem.*, 2012, **22**, 19658–19665.
40 Z. X. Liang, T. S. Zhao, J. B. Xu and L. D. Zhu, *Electrochim. Acta*, 2009, **54**, 2203–2208.
41 R. C. Cerritos, M. Guerra-Balcázar, R. F. Ramírez, J. Ledesma-García and L. G. Arriaga, *Materials*, 2012, **5**, 1686–1697.
42 Z. P. Guo, D. M. Han, D. Wexler, R. Zeng and H. K. Liu, *Electrochim. Acta*, 2008, **53**, 6410–6416.

 This journal is © The Royal Society of Chemistry 2015